

# Ultrafast Field-Emission Electron Sources Based on Nanomaterials

Shenghan Zhou, Ke Chen, Matthew Thomas Cole, Zhenjun Li, Jun Chen, Chi Li,\*  
and Qing Dai\*

The search for electron sources with simultaneous optimal spatial and temporal resolution has become an area of intense activity for a wide variety of applications in the emerging fields of lightwave electronics and attosecond science. Most recently, increasing efforts are focused on the investigation of ultrafast field-emission phenomena of nanomaterials, which not only are fascinating from a fundamental scientific point of view, but also are of interest for a range of potential applications. Here, the current state-of-the-art in ultrafast field-emission, particularly sub-optical-cycle field emission, based on various nanostructures (e.g., metallic nanotips, carbon nanotubes) is reviewed. A number of promising nanomaterials and possible future research directions are also established.

## 1. Introduction

Electron sources are the core component of various widely adopted systems, ranging from those used in medical diagnosis to systems applied to homeland security. The first generation of vacuum electronic devices were thermionic sources, which continue to dominate the market more than a century after their inception. As new materials continue to rapidly emerge, over the past few decades, the electron emission community has shifted its focus to cold-cathode field emission.<sup>[1]</sup> Field-induced electron emission is the quantum mechanical tunneling of electrons through a material-dependent potential barrier under the influence of a high electric field. The absence of a solid-state

transport channel and the intrinsically ultrafast response time [on the order of attoseconds ( $10^{-18}$  s)] allow near-instantaneous emission. As a result, there is considerable interest in the use of field-emission electron sources in various vacuum electronic applications, such as flat-panel displays,<sup>[2]</sup> microwave amplifiers,<sup>[3]</sup> electron microscopes,<sup>[4]</sup> and X-ray sources.<sup>[5]</sup> The successful demonstration of a variety of field-emission instruments is a highly significant milestone that may ultimately lead to a combined spatial and temporal resolution that is yet to be achieved using other technologies. The pursuit of a high-performance field-emission source relies inti-

mately on advanced materials engineering.<sup>[6]</sup> Nanomaterials have already demonstrated superior field-emission performance to that of their bulk counterparts.<sup>[7]</sup> The distinctive electronic structures and nanometric emitting surfaces of these new materials provide extremely high field-enhancement factors.<sup>[8]</sup> Today, the use of nanomaterials enables devices that simply could not have been manufactured only a decade or so ago.


However, the advantageous bifunctionality of field emission—extremely high spatial and correspondingly high temporal resolution—has yet to be fully realized. In the past decade, motivated by attosecond science at a sub-nanometer scale,<sup>[9,43]</sup> together with the drive toward ultrafast electron microscopy,<sup>[10]</sup> next-generation field-emission electron sources with both sub-nanometer spatial resolution and attosecond temporal resolution have gained great attention.<sup>[11]</sup> On the one hand, there is still a need for research on further enhancement in the spatial resolution, which is typically achieved through the coupling of advanced transport physics with state-of-the-art materials science. By embracing bottom-up, atom-by-atom synthesis of new 1D<sup>[12]</sup> and 2D<sup>[13–15]</sup> materials, the ultimate aim of engineering truly single-atom-scale emission sites is appearing increasingly achievable. On the other hand, it is somewhat challenging to improve temporal resolution through the use of conventional electronics. New excitation methodologies are essential to reach femto- and even attosecond time scales. Excitation by ultrashort strong electromagnetic fields of light is one viable approach.<sup>[16,17]</sup> It is this continuing pursuit of high temporal resolution field emission that has triggered the emergence of a new discipline: lightwave electronics,<sup>[18]</sup> whose central tenet is the investigation and control of dynamic electron transport at sub-optical-cycle time scales.

Here, we capture the present state of this emerging field. We first briefly review the methodologies of ultrafast field emission,

S. H. Zhou, K. Chen, Dr. M. T. Cole, Dr. Z. J. Li, Prof. J. Chen,  
Dr. C. Li, Prof. Q. Dai  
Division of Nanophotonics  
CAS Center for Excellence in Nanoscience  
National Center for Nanoscience and Technology  
Beijing 100190, China  
E-mail: lich@nanoctr.cn; daiq@nanoctr.cn

S. H. Zhou, K. Chen, Dr. M. T. Cole, Dr. Z. J. Li,  
Prof. J. Chen, Dr. C. Li, Prof. Q. Dai  
University of Chinese  
Academy of Sciences  
Beijing 100049, P. R. China

Prof. J. Chen  
State Key Laboratory of Optoelectronic Materials and Technologies  
Guangdong Province Key Laboratory of Display Material and Technology  
School of Electronics and Information Technology  
Sun Yat-sen University  
Guangzhou 510275, China

 The ORCID identification number(s) for the author(s) of this article can be found under <https://doi.org/10.1002/adma.201805845>.

DOI: 10.1002/adma.201805845

including electric field and strong optical field interactions. Then, we turn to the current development of ultrafast field-emission electron sources and their applications, focusing on recent developments in optical field electron emission, based mainly on metal nanostructures, alongside our recent progress on carbon nanotube (CNT) ultrafast field emitters. We then summarize the materials of interest in ultrafast field emission. Herein, we aim to bridge the disciplines of conventional quasi-static field-emission research and emerging ultrafast optical field-emission research.

## 2. Ultrafast Field-Emission Methodology

### 2.1. Fundamentals of Field Emission

Under a high electric field, the vacuum level at the surface of an emitter bends downward, and a triangular barrier is thus formed. Field electron emission is the quantum tunneling of electrons through such a narrow potential barrier into a vacuum (Figure 1A). This phenomenon was first modeled by Fowler and Nordheim in 1928,<sup>[19]</sup> who found that the emission current density  $J$  depends on the electric field strength  $E$ , the field-enhancement factor  $\beta$ , and the work function  $\Phi$  of the material. It takes the following form, commonly termed the Fowler–Nordheim (FN) equation

$$J = \frac{C_1 (\beta E)^2}{\Phi} \exp\left(-\frac{C_2 \Phi^3}{\beta E}\right) \quad (1)$$

where  $C_1 = \frac{e^3}{8\pi h}$  and  $C_2 = \frac{8\pi\sqrt{2m}}{3he}$  are the basic constants (the charge and mass of an electron are denoted by  $e$  and  $m$ , respectively, and the Planck constant is  $h$ ). Clearly,  $\Phi$  and  $\beta$  dominate the field-emission characteristics of the emitting materials. Thus, a common methodology for optimizing the emitter and discovering new materials has been to decrease the  $\Phi$  and regulate the external morphology of the material to increase the  $\beta$ .



**Chi Li** is an associate professor in the National Center of Nanoscience and Technology, China. He received his Ph.D. in physics electronics from the School of Electronic Science & Engineering, Southeast University in 2011. His main research interests are low-dimensional materials, optoelectronics, and nanophotonics.



**Qing Dai** is a professor in the National Center of Nanoscience and Technology, China. He received his M.Eng. in electronic and electrical engineering from Imperial College, London, in 2007 and his Ph.D. in nanophotonics from the Department of Engineering, University of Cambridge in 2011. His main research

interests are low-dimensional materials, optoelectronics, and nanophotonics.

### 2.2. Ultrafast Laser-Assisted Electric Field Emission

Laser-assisted electric field emission has recently been applied to improve field-emission performance. The underlying mechanism includes thermal-field emission<sup>[20]</sup> and photofield emission (PFE).<sup>[21]</sup> Under these regimes, electrons are first excited from their original energy level to a higher energy-level state by absorbing thermal or photon energy (Figure 1B). They

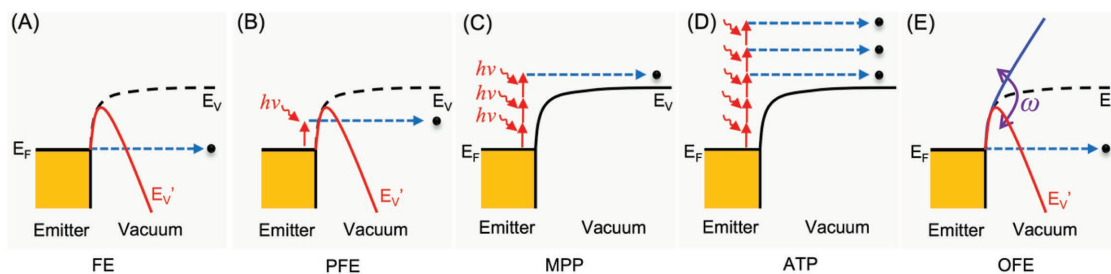


**Figure 1.** Mechanisms of electron emission. A) Field emission (FE). The quantum tunneling of electrons through an electric field-induced narrow potential barrier into vacuum.  $E_F$ , Fermi level.  $E_V$ , original vacuum level.  $E_V'$ , bent vacuum level under an electric field. B) Photofield emission (PFE). An electron is excited to an intermediate state at a higher energy level than its original energy level ( $E_F$ ) when gaining the energy of a photon and tunnels through a much narrower barrier. C) Multiphoton photoemission (MPP). An electron absorbs the energy of a number of photons to overcome the vacuum barrier for photoemission. D) Above-threshold photoemission (ATP). In a multiphoton regime, more than the minimum required number of photons can be absorbed for photoemission. E) Optical field emission (OFE). A strong optical field induces a periodically varying vacuum level with an optical frequency ( $\omega$ ). When the optical field is strong enough to create a penetrable tunneling barrier, electrons tunnel from the Fermi level in a fraction of a negative half optical-cycle.

then face a much narrower tunneling barrier, meaning that the tunneling probability is greatly increased, which results in a highly enhanced emission current. The laser-assisted emission from nanostructures can be analyzed in the framework of the two-temperature model,<sup>[22]</sup> which describes the experimental results in terms of coupling between electron and lattice systems. Upon irradiation of the emitter material with an intense laser, the energy of the photons is transferred to the electrons, creating an ensemble of hot electrons. The hot electrons then exchange their energy with the lattice.

Conventional energy-assisted electric field emission made use of electrical heating or continuous-wave laser exposure to provide this additional energy. However, such excitation methodologies do not allow femtosecond response times. Ultrafast femtosecond laser-assisted electric field-emission is considered the primary candidate method for retaining the ultrafast nature of field emission.<sup>[23]</sup> When excited by exposure to ultrafast laser pulses, electrons may be excited to nonequilibrium states by obtaining energy from both photons and thermal (laser-heating) effects. In the case of photon-driven excitation, the time scale of the general electron pulse is the same as that of the laser pulse.<sup>[24]</sup> In the case of thermally driven excitation, time frames of >100 fs are required to transfer sufficient thermal energy to the local electron population.<sup>[25]</sup>

### 2.3. Ultrafast Optical Field Emission

Upon illumination with an intense femtosecond laser pulse, the electrons in a material may absorb more than one photon, which is known as multiphoton absorption. Such a regime enables photoemission under incident light with a photon energy smaller than the work function of the emitting surface, which is known as multiphoton photoemission. In the multiphoton photoemission regime (Figure 1C), the minimum number  $n$  of energy quanta  $\hbar\nu$  required to overcome the work function is absorbed by the emitting surface ( $\hbar$  is the reduced Planck constant). The photocurrent follows a power law of the form  $P^n$ , where  $P$  refers to the laser power and the exponent  $n$  refers to the number of photons absorbed. In this multiphoton scheme, more than the minimum required number of photons can be absorbed, referred to as above-threshold multiphoton photoemission<sup>[26]</sup> (Figure 1D). The time scale of the multiphoton photoemission is the same as the width of the laser pulse.

Much faster electron emission can be achieved through optical field emission (OFE).<sup>[27]</sup> OFE is a type of strong-field photoemission regime in which the electric field (optical field) of the incident light is strong enough to induce a periodically varying surface vacuum level, as shown in Figure 1E. With a sufficiently strong optical field, electrons can tunnel through the narrow barrier from states in the vicinity of the Fermi level during a fraction of the negative half optical cycle. OFE can thus produce sub-optical-cycle duration electron pulses. Photoemission may transition into OFE from a conventional photon-driven regime with increasing optical field strength. The transition can be described by the Keldysh framework,<sup>[28]</sup> which was originally formulated for the strong-field ionization of gas-phase atoms and molecules and subsequently extended

to strong-field photoemission from a solid surface.<sup>[29]</sup> The Keldysh framework introduces a characteristic parameter  $\gamma$  that separates two limiting regimes, a multiphoton photoemission regime<sup>[30]</sup> ( $\gamma > 1$ ) and a tunneling emission regime ( $\gamma < 1$ ). The latter is termed OFE. The Keldysh parameter  $\gamma$  is given by  $\gamma = \omega \sqrt{2m\phi} / e\beta F$ , where  $\omega$  is the optical frequency;  $\phi$  is the work function;  $m$  and  $e$  are the mass and charge of the electron, respectively;  $F$  is the incident light-field strength; and  $\beta$  is the field-enhancement factor of the emitting tips.

### 2.4. Advantages of Nanomaterials

To date, much of the research on field emission has relied on advances in materials technology, especially those related to the growth of nanomaterials. Ever-increasing field-enhancement factors and ever smaller work functions have proven essential to these advances, both of which lower the external electric field and associated laser intensity required for excitation. The search for smaller emitting tips fabricated from exotic materials has thus been intense. The need for longevity and brightness also implies the need for additional material properties, such as high mechanical strength and low chemical reactivity, if such emitters are to operate successfully under extreme conditions.

According to the Keldysh parameter ( $\gamma$ ), to gain access to OFE, a very high optical field strength is required. However, this objective is limited by both the damage threshold of the material and the available power of the laser. Thus, the optical near-field-enhancement factor  $\beta$  of the emitter material plays a key role; for 1D nanomaterials, this factor is mostly derived from the lightning rod effect induced by the sharp tips, which also exists in static field emission.<sup>[31]</sup> At nanoscale discontinuities, such as at nanotips and nanorods, the electron density is notably very high, which induces a considerable near-field enhancement. Exploiting localized surface plasmons (LSPs) have proven a useful means of photoelectron excitation and is a secondary mechanism in near-field enhancement.<sup>[32]</sup> With resonant optical excitation, the system naturally leads to higher field enhancement than other mechanisms operating in non-plasmonic materials.<sup>[33]</sup>

### 2.5. Experimental Methods

Intense femtosecond laser exposure is required to achieve OFE due to the extremely high incident optical field strength. Normally, a local optical field strength of  $\approx 20 \text{ V nm}^{-1}$  at the emitting surface is necessary to access the OFE regime. For emitters with a high field-enhancement factor, the laser-pulse intensity generated by comparatively inexpensive ultrafast oscillators has proven sufficient to achieve such a regime.<sup>[34]</sup> However, if the field-enhancement factor of the emitter is relatively low, ultrafast amplifiers are required;<sup>[17]</sup> these amplifiers can normally output an enhanced optical field 2–3 orders of magnitude higher than that output by an ultrafast oscillator. The maximum photoemission current occurs when the optical polarization is parallel to the axis of the emitting tip. To collect the liberated electrons, a static electric (DC) field is commonly applied

between the tips, and an electron collection electrode is placed in their proximity. Notably, this DC field must be moderately low to avoid DC electric field emission. The photoemission electron yield can be measured by a high-precision digital source meter or counted by an electron multiplier plate.<sup>[17]</sup> The emission image can be monitored by a phosphor screen,<sup>[35]</sup> which can be read both electronically and by a timed and triggered charge-coupled device (CCD) camera.<sup>[35]</sup> Finally, the energy distribution of the liberated electrons can be measured using, for example, a retarding field grid energy analyzer, time-of-flight spectrometer,<sup>[36]</sup> or hemispherical energy analyzer.<sup>[37]</sup> The retarding field grid analyzer and time-of-flight spectrometer can achieve an energy resolution of a few tens of meV, while the hemispherical energy analyzer can reach a high resolution of a few meV.

OFE from nanotips is driven by the optical carrier waveform (electric field) of the laser pulses rather than its envelope. To examine such behavior, careful control of the temporal evolution of the electric field of the laser pulses is required.<sup>[38]</sup> Accordingly, ultrashort few-cycle pulses with control of their carrier-envelope phase (CEP) are frequently used. The CEP of a laser pulse is the phase between the carrier wave (electric field) and its intensity envelope.<sup>[39]</sup> In a few-cycle laser pulse, the peak electric field of half-cycles (negative cycles or positive cycles) can be sensitively controlled by tuning the CEP. For a nanotip emitter, OFE occurs only in half-cycles of the laser pulse when the electric field direction is consistent with the tip orientation. The method exploits the exponential sensitivity of the emission probability to the field amplitude in combination with symmetry breaking at the emitting surface. CEP effects in photoemission can be used as a CEP detector<sup>[38,40]</sup> and as a means of revealing the sub-optical-cycle dynamics of the photoemission process.<sup>[41]</sup>

### 3. State-of-the-Art Ultrafast Field-Emission Sources

Research on ultrafast field emission, especially OFE, has attracted a considerable amount of interest, leading to significant progress over the past decade.<sup>[39]</sup> In an OFE regime, electrons are liberated in a fraction of an optical cycle. Therefore, by employing near-infrared or visible laser pulses, attosecond temporal resolution electron pulses are generated with a high degree of synchronization with the incident optical waveform.<sup>[42]</sup> This development not only advances time-resolved electron characterization into an attosecond time domain but also provides an attosecond control and measurement methodology.<sup>[43]</sup> Thus, OFE is at the core of various modern attosecond technologies, such as attosecond electron microscopy,<sup>[44]</sup> petahertz electronic devices,<sup>[45,46]</sup> attosecond light sources,<sup>[47]</sup> and optical-phase detectors.<sup>[48]</sup>

To date, OFE experiments have been conducted with many nanomaterials, including metal nanostructures, carbon nanomaterials, Si nanotips, and nanodielectrics, due to their two intimately connected features—local laser intensity enhancement and subwavelength confinement of optical fields. **Table 1** summarizes typical OFE materials and their key parameters. This section presents the current state-of-the-art in nanostructure-based ultrafast field-emission sources.

#### 3.1. Metallic Nanostructures

Metal nanostructures, such as nanotips,<sup>[17]</sup> nanowires,<sup>[49]</sup> nanospheres,<sup>[50]</sup> nanorods,<sup>[60,51,52]</sup> nanotriangles,<sup>[53]</sup> nanostars,<sup>[61]</sup> and composite bow-tie and nanorod antennae,<sup>[36,45b,53,62]</sup> are of particular interest for OFE experiments due to their relatively

**Table 1.** Typical ultrafast field-emission materials and their key parameters.

Materials	Morphology	Size of the emitting tip	Substrate	Field enhancement (wavelength)	Dominant field-enhancement mechanism	The local optical field strength (when accessing strong field emission)
Gold	Nanowire <sup>[49]</sup>	90–190 nm <sup>[49]</sup>	Tungsten tips <sup>[49]</sup>	Simulation: 6.6–10.4 (750 nm) <sup>[49]</sup> Experiment: 5.98 ± 0.24 (750 nm) <sup>[49]</sup>	Geometry effect <sup>[49]</sup>	23 V nm <sup>-1</sup> <sup>[49]</sup>
	Nanosphere <sup>[50]</sup>	90 nm <sup>[50]</sup>	Si <sup>[50]</sup>	1000 (780 nm) <sup>[50]</sup>	Plasmon resonance <sup>[50]</sup>	50 V nm <sup>-1</sup> <sup>[50]</sup>
	Nanorod <sup>[51,52]</sup>	150 nm × 50 nm <sup>[51]</sup> 70 nm × 20 nm <sup>[52]</sup>	ZnS <sup>[51]</sup>	36 (500 nm) <sup>[51]</sup>	Plasmon resonance <sup>[51,52]</sup>	3.5 V nm <sup>-1</sup> <sup>[51]</sup>
			ITO <sup>[52]</sup>	60 (800 nm) <sup>[52]</sup>		3–4.3 V nm <sup>-1</sup> <sup>[52]</sup>
	Nanotip <sup>[17]</sup>	10 nm <sup>[17]</sup>	–	10 (800 nm) <sup>[17]</sup>	Plasmon resonance and geometry effect <sup>[17]</sup>	28 V nm <sup>-1</sup> <sup>[17]</sup>
Nanotriangle <sup>[53]</sup>	(160–300 nm × 120–225 nm) <sup>[53]</sup>	ITO <sup>[53]</sup>	32 (1177 nm) <sup>[53]</sup>	Plasmon resonance <sup>[53]</sup>	40 V nm <sup>-1</sup> <sup>[53]</sup>	
Tungsten	Nanotip <sup>[54,55]</sup>	5 nm <sup>[54]</sup>	–	12 (800 nm) <sup>[54]</sup>	Geometry effect <sup>[54,55]</sup>	–
		8–51 nm <sup>[55]</sup>	–	2.6–5.7 (800 nm) <sup>[55]</sup>		8.7 V nm <sup>-1</sup> <sup>[55]</sup>
Silicon	Pillar <sup>[56]</sup>	4.4 nm <sup>[56]</sup>	–	10.5 (800 nm) <sup>[56]</sup>	Geometry effect <sup>[56]</sup>	8.7 V nm <sup>-1</sup> <sup>[56]</sup>
Silver	Nanotip <sup>[57]</sup>	12–50 nm <sup>[57]</sup>	–	3.8 ± 0.1 (800 nm) <sup>[57]</sup> 12.2 ± 2 (400 nm) <sup>[57]</sup>	Plasmon resonance and geometry effect <sup>[57]</sup>	2.7 V nm <sup>-1</sup> <sup>[57]</sup>
Dielectric	Nanosphere <sup>[58,59]</sup>	100 nm <sup>[59]</sup>	–	1.3 (720 nm) <sup>[59]</sup>	Geometry effect <sup>[58,59]</sup>	15 V nm <sup>-1</sup> <sup>[59]</sup>
		52–147 nm <sup>[58]</sup>	–	1.54 (720 nm) <sup>[58]</sup>		12.3 V nm <sup>-1</sup> <sup>[58]</sup>
Carbon nanotube	Nanotip <sup>[34]</sup>	0.5–1 nm <sup>[34]</sup>	–	26.7 ± 0.5 (410 nm) <sup>[34]</sup>	Geometry effect <sup>[34]</sup>	0.66 V nm <sup>-1</sup> <sup>[34]</sup>

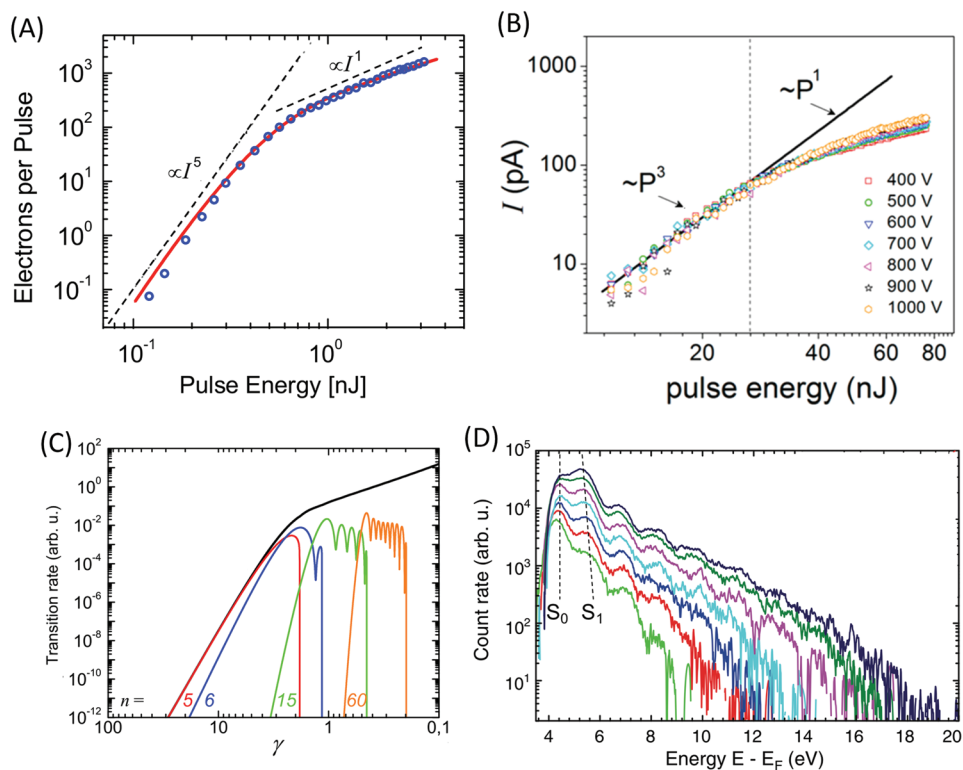


**Figure 2.** Access to the OFE regime. A) Measured number of emitted electrons as a function of pulse energy (circles), referred to as the  $I$ - $P$  curve, from an Au nanopip. A “kink” is observed at a pulse energy of  $\approx 0.4$  nJ. The  $I$ - $P$  curve calculated using a strong-field approximation model [solid (red)] fits well with the measured data.<sup>[35]</sup> B) Measured  $I$ - $P$  curve of a  $1 \mu\text{m}$  pitch square array of Au nanorod emitters at different applied anode bias values. A “kink” is observed at a pulse energy of  $\approx 26$  nJ.<sup>[64]</sup> C) Theoretically calculated transition rate of a single channel [gray lines, marked  $n = 5, 6, \dots$ ] and total sum (black line) as a function of  $\gamma$ . The calculation reveals that the “kinks” are a result of the channel-closing effect when the laser intensity increases ( $\gamma$  decreases).<sup>[35]</sup> D) Experimentally obtained electron count rate as a function of the electron energy.<sup>[65]</sup> From bottom to top, the curves are taken at increased laser intensities. The third-order photoelectron peak ( $S_0$ ) is suppressed (channel-closing) when the laser intensity increases, while the higher-order peaks [only the fourth-order peak ( $S_1$ ) is marked] shift to lower energy positions. These experimental observations provide evidence for the theoretical calculation (shown in (C)). (A,C) Reproduced with permission.<sup>[35]</sup> Copyright 2010, APS; (B) Reproduced with permission.<sup>[64]</sup> Copyright 2014, American Chemical Society; (D) Reproduced with permission.<sup>[65]</sup> Copyright 2010, APS.

simple electronic structures and strong plasmonic near-field enhancement. Many novel electron dynamics phenomena have been discovered during the investigation of OFE from metallic tips in this way. Metallic nanopip tips have already been applied in various practical devices, such as in ultrafast electron microscopy. In this section, we briefly review the novel electron dynamics observed on metal tips and their current application in ultrafast electron sources.

Recent research has demonstrated OFE from nanopip tips during short-wavelength ( $< 800$  nm) excitation. The transition to OFE was indicated by strong deviations in the photoemission transport profiles from the multiphoton photoemission power law,<sup>[35,63,64]</sup> marked by a sharp “kink” observed in the current-intensity ( $I$ - $P$ ) curve, as shown in **Figure 2A,B**. However, such transitions are often observed at  $1 < \gamma < 2$ . This behavior is inconsistent with Keldysh theory,<sup>[28]</sup> which predicts pure OFE at  $\gamma \ll 1$ . A hybrid photoemission regime—strong-field above-threshold photoemission—is now widely accepted. At higher intensities, the strong optical field effect becomes increasingly dominant at the vacuum barrier, which results in closure of the multiphoton photoemission channel.<sup>[66]</sup> This effect has been successfully modeled in the framework

of time-dependent perturbation theory using a strong-field approximation by solving the time-dependent Schrödinger equation (Figure 2C).<sup>[35]</sup> It was then experimentally confirmed by electron spectroscopy that a strong optical field shifts the high-order photoelectron peaks to lower kinetic energies together with closure of the low-order channels,<sup>[16]</sup> as shown in Figure 2D. Further channel-closing leads to a pronounced decrease in the nonlinearity of the photoemission—compared with that in the multiphoton regime, the photoemission current in this regime shows a relatively low order of the power law (power order  $n \approx 1$ ) of the laser intensity.<sup>[35]</sup> Such a phenomenon has also been observed at arrays of n-doped Si tips (800 nm),<sup>[56]</sup> Au nanoarrays (800 nm),<sup>[67]</sup> Au nanoarray devices,<sup>[53]</sup> and CNTs (800 nm, 400 nm).<sup>[34,68]</sup>

A novel type of quiver-quenched electron dynamics was discovered in the OFE from an Au nanopip.<sup>[17]</sup> After tunneling into continuous states (first step), electrons are accelerated in a strong optical near-field (second step). This so-called two-step Simpleman model captures the otherwise complex dynamics in a simplified form.<sup>[69]</sup> Despite its simplicity, this model is capable of accurately describing various experimental observations. In the oscillating optical near-field, the electrons



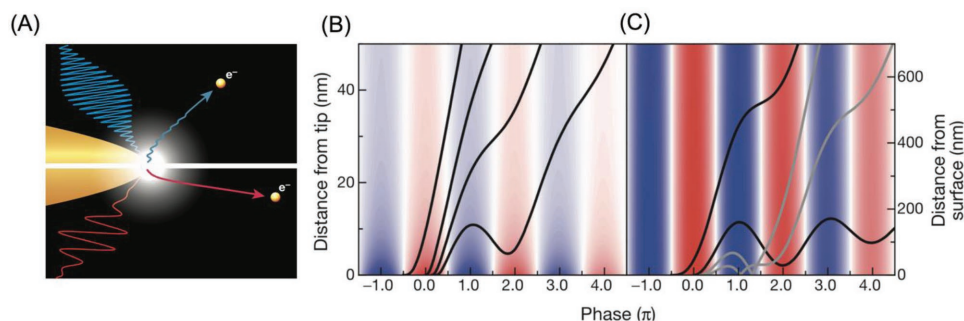


**Figure 3.** Sub-optical-cycle acceleration regime. A) Trajectories of photoelectrons generated by intense optical fields depend strongly on whether the quiver amplitude is smaller (top, short-wavelength excitation) or larger (bottom, long-wavelength excitation) than the characteristic decay length of the optical near-field (bright white region). B,C) Simulated electron trajectories for four emission phases in localized and homogeneous pulsed fields (wavelength 8 nm; color shading indicates field; the red and blue indicate positive and negative electric force on electrons, respectively). The gray lines are rescattered trajectories. (A–C) Reproduced with permission.<sup>[17]</sup> Copyright 2012, Nature Publishing Group.

have a typical quiver amplitude of  $l_q = eF/m\omega^2$ . In the case of nanoscale tips, the optical field decays exponentially with the distance from the tip surface, with a decay length  $l_F$  that is proportional to the tip radius. The electron trajectory is described by a spatial adiabaticity parameter ( $\delta = l_F/l_q$ ).<sup>[17]</sup> For  $\delta \gg 1$ , most of the electrons quiver in the optical field, accompanied by strong surface rescattering, termed the “quiver regime” (upper panel of Figure 3A,C). For  $\delta < 1$ , most of the emitting electrons escape the local optical field in one optical cycle, with minimal quiver and rescattering, termed the “sub-cycle regime” (lower panels of Figure 3A,B). The first observation of sub-optical-cycle acceleration in a nanotip near-field was presented by Ropers and co-workers.<sup>[17]</sup> The effect was further investigated in a systematic study by Echternkamp et al.<sup>[70]</sup> on a W tip. Because sub-optical-cycle OFE avoids the time delay in a quiver regime,<sup>[71]</sup> it thus encodes the instantaneous optical field onto the electron energy. The locally accelerated electrons have excellent spatial coherence, which is critical for next-generation ultrafast electron sources.

OFE from metals has been theoretically predicted to be very sensitive to the CEP.<sup>[72]</sup> However, in reality, a much lower CEP modulation effect on the total photoemission current has been observed.<sup>[73,74]</sup> This inconsistency is believed to be due to the limited optical field modulation efficiency that results from the reduced photoemission nonlinearity<sup>[74]</sup> (i.e., the power order of the  $I$ – $P$  curve, as discussed above). The low modulation sensitivity may ultimately limit practical applications, such as in CEP detectors.<sup>[53]</sup> To address this issue, the electron kinetic energy spectrum of the OFE from W tips was recently investigated and was discovered to be more sensitive to the CEP. As reported by Hommelhoff and co-workers,<sup>[16]</sup> two strong optical field effects—the suppression of low-order photoelectron peaks (Figure 2E) and the plateau in the high energy part of the spectrum (Figure 4A)—are observed, both of which are strongly dependent on the driving carrier-field waveform of the pulses. It is thus clear that spectral profiles can be strongly modulated by the CEP (Figure 4B). Notably, the modulation depths of the peak at the cutoff position reached up to 100% (Figure 4A), which is more sensitive than the modulation of the total photoemission current (up to  $\approx 50\%$ ).<sup>[74]</sup>

Due to the extremely high temporal resolution, metallic tips have been applied as ultrafast field-emission electron sources

in femtosecond point-projection microscopy (fsPPM),<sup>[75,76]</sup> ultrafast low-energy electron diffraction (ULEED),<sup>[77]</sup> and the combination of these two technologies.<sup>[78]</sup> This development has extended the temporal resolution of electron microscopy to the picosecond and even to the femtosecond scale; however, the spatial resolution is limited to the order of a hundred micrometers. In 2013, Barwick and co-workers<sup>[75]</sup> introduced a nanometer ultrafast electron source into point-projection microscopy. They demonstrated a spatial resolution of 100 nm. If the spatial resolution can be further reduced, it may replace traditional expensive and complicated electron microscopy systems. Subsequently, Gulde et al.<sup>[77]</sup> used W nanotips to develop a unique ULEED system with extremely high surface sensitivity to detect the surface structure of crystalline materials. Muller et al.<sup>[78]</sup> designed a compact hybrid device that combines fsPPM with femtosecond low-energy electron diffraction (fsLEED). The microscale electron propagation distance greatly reduces electron pulse broadening, while using a single electron pulse allows a temporal resolution of femtoseconds to be achieved.

### 3.2. Carbon Nanotubes

Based on the understanding of ultrafast field-emission phenomena from metallic tips, research efforts have now been extended to other materials in an attempt to more fully exploit their advantages. One promising class of materials is CNTs. Since their discovery, CNTs have gained much attention in a wide range of applications, especially as electron sources. These robust 1D materials are near-ideal field electron emitters. A CNT may have an aspect ratio as high as 1000, 10–100 times greater than that of an equivalent metallic emitter, which results in a very high field-enhancement factor. The enhancement facilitated by CNTs is mostly based on geometrical effects due to their extremely small tip radius. They thus possess a high optical field-enhancement effect under a much greater bandwidth. Recently, the OFE performance of CNTs was investigated (Figure 5A). The tip radius of the CNTs used was  $\approx 1$  nm (Figure 5B,C). For the first time, the OFE regime was accessed at a much shorter wavelength of 410 nm (Figure 5D), which was never achieved with previous metallic nanotips. This

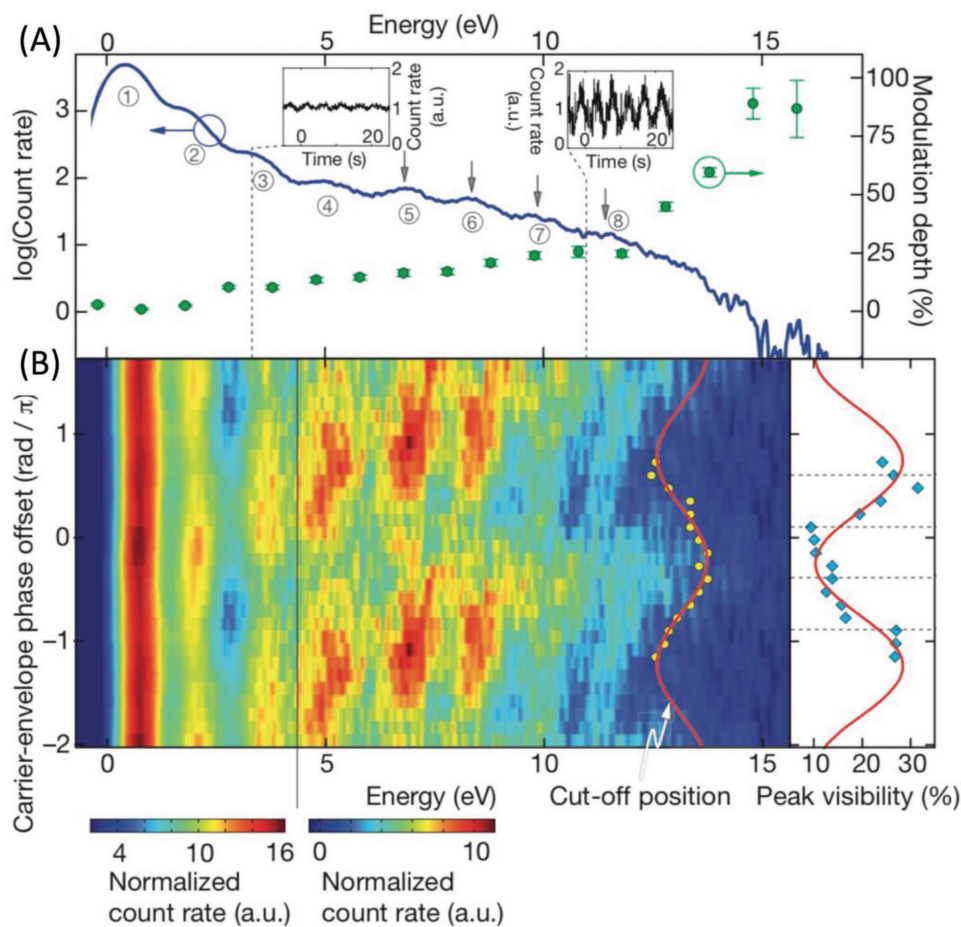


**Figure 4.** Carrier-envelope phase (CEP) modulation in photoelectron spectra. A) CEP-averaged electron count rate as a function of energy (solid line). The electrons with different photon orders are marked by ①, ②, ③.... For energy > 4.5 eV, the plateau region starts with five more photon orders visible. The green points depict the modulation depth of the count rate when varying the CEP. B) Contour plot of the electron count rate as a function of CEP offset and energy. The yellow circles show the position of the cutoff for a given CEP offset (red curve, sinusoidal fit). Right-hand panel, average peak visibility (blue dots) in the plateau region (red curve, sinusoidal fit). The peaks used to determine the visibility are marked with gray arrows in (A). All panels reproduced with permission.<sup>[16]</sup> Copyright 2011, Nature Publishing Group.

result is a benefit of the very high enhancement factor of  $\approx 27$  at 410 nm<sup>[34]</sup> (Figure 5E). In addition, the emitted electrons have great monochromaticity with an energy spread as low as 0.25 eV (Figure 5F).

In addition, CNTs with sub-nanometer tip radii have an extremely small field decay length (<0.4 nm), which allows easier access to quiver-quenched electron dynamics in the OFE regime. However, the  $\delta$ -parameter is inversely proportional to the optical field ( $F$ ) for a fixed wavelength, which suggests higher laser intensity is required to access a subcycle regime. Because the experimentally accessible intensity range is limited by damage thresholds, access to a subcycle regime by increasing  $F$  is expected to be somewhat less pronounced, especially for short-wavelength laser pulses. Fortunately, compared with conventional metal tips, CNT emitters have a much higher  $\beta$  and a much smaller  $R$ , as well as a significantly greater damage threshold, all of which facilitate improved access to the subcycle regime.<sup>[68]</sup> In a recent OFE experiment with CNTs<sup>[68]</sup> using 820 nm laser pulses,  $\delta$  was decreased to a low value of  $\approx 0.53$  with increasing laser power. This result suggests that the

OFE effectively accessed the subcycle regime, which is supported by the fact that the cutoff energy increases sublinearly with the optical field strength.<sup>[68]</sup> These demonstrations offer exciting prospects for extending the current characterization techniques to both sub-femtosecond temporal resolutions and sub-nanometer spatial resolutions.

### 3.3. Other Nanostructure Ultrafast Field Emitters

In addition to metallic structures and CNTs, silicon nanotip arrays,<sup>[56]</sup> dielectric nanospheres,<sup>[58,79,59,80]</sup> and C<sub>60</sub> buckyballs<sup>[81]</sup> have also been used in ultrafast field-emission experiments. For example, Swanwick et al.<sup>[56]</sup> designed arrays of nanosharp silicon pillars as a novel ultrafast field emitter. The field enhancement of the high-aspect-ratio silicon tip array resulted in achieving OFE at low power ( $\approx 0.2 \mu\text{J}$ ). These emitter arrays are highly dense and uniform and can produce a confined structured ultrafast electron beam. C<sub>60</sub> is an ideal system for achieving OFE because it is very

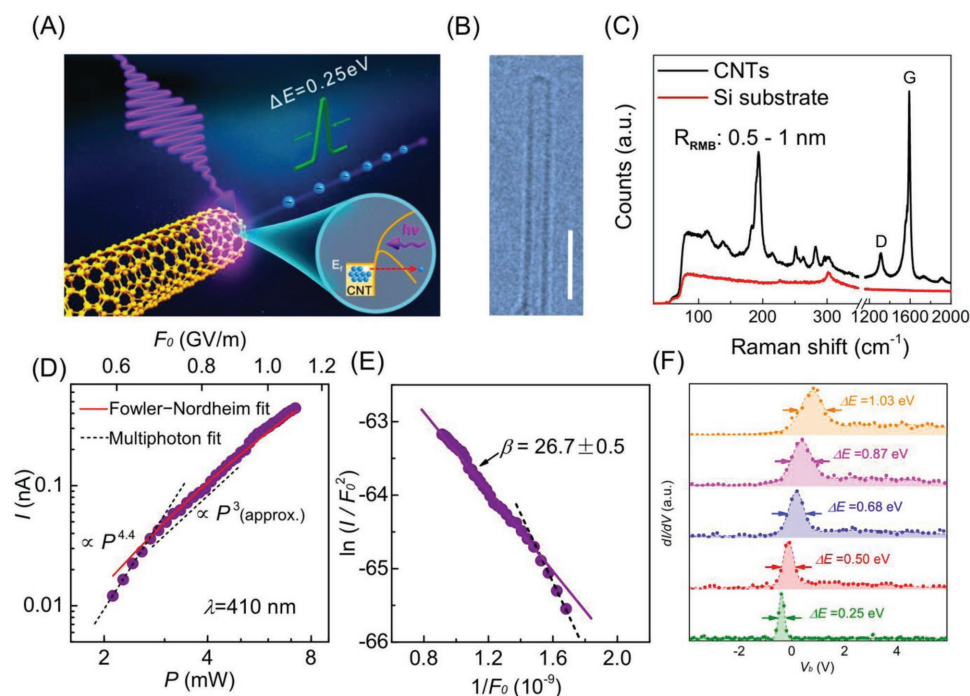


**Figure 5.** CNT-based ultrafast OFE source. A) Emission dynamics. B) High-resolution transmission electron microscopy image of a typical CNT under study. Scale bar: 5 nm. C) Raman spectrum of CNTs, which indicates a radius of 0.5–1 nm. D) Emission current as a function of laser power ( $P$ ) (bottom abscissa) and laser field ( $F_0$ ) (top abscissa) at a bias voltage ( $V_b$ ) of 50 V. In the low-power range, a multiphoton regime is noted, while access to the OFE regime is noted in the higher power range. E) Fowler–Nordheim (FN) plot of the optically driven emission current, showing a field-enhancement factor ( $\beta$ ) of  $26.7 \pm 0.5$ . F) Corresponding  $dI/dV$  curves. The width of the peaks (FWHM) indicates the energy spreads ( $\Delta E$ ), while the shoulder indicates the beam divergence grade. (A–E) Reproduced with permission.<sup>[34]</sup> Copyright 2015, Wiley-VCH.

stable and is one of the few molecular systems for which the ionization energy is less than the lowest fragmentation threshold.<sup>[81]</sup> Li et al.<sup>[81]</sup> reported OFE from  $C_{60}$  using few-cycle laser pulses and demonstrated sensitive CEP modulation of the photoemission current. Dielectric nanospheres have a relatively wide spectral response, allowing them to use the full bandwidth of ultrashort pulses. Therefore, many studies have focused on dielectric nanospheres, including attosecond control of collective electron motion,<sup>[58]</sup> electron scattering in strong-field photoemission,<sup>[59,80]</sup> and CEP-controlled photoemission.<sup>[79]</sup>

#### 4. Potential Ultrafast Field-Emission Materials

There is currently a notable trend in the use of increasingly more exotic nanomaterials to investigate ultrafast field emission. In addition to the higher optical field-enhancement factors of such materials, their potentially lower work functions are also favorable for reducing the high optical field required. In this section, we summarize the suitability and use of several potential nanomaterials as ultrafast field emitters.

##### 4.1. Wide-Bandgap Semiconductors

In the search for appropriate materials for field emission, diamond thin films were discovered in the early 1990s.<sup>[82]</sup> These materials

have attracted significant attention, with many thousands of reports having been published to date. In addition to having low and even negative surface electron affinity,<sup>[83]</sup> diamond and related films are especially attractive emission platforms because they are chemically inert and have extremely high thermal conductivity and mechanical toughness. They therefore represent an excellent candidate for ultrafast field emission. However, due to their growth by nominally planar chemical vapor deposition methods, these films have relatively low field-enhancement factors, severely compromising their emission performance. Subsequently, diamond films or nanoparticles<sup>[84]</sup> have also been synthesized on other micro-nanotips to enhance the field-emission properties of uncoated materials.<sup>[85]</sup> Recently, nanosecond laser-assisted field emission from a diamond needle was investigated.<sup>[86]</sup> The photoinduced emission current was attributed to the ionization of the excitons in the bulk and subsequent transport of generated hot electrons to the emission point. This work suggests that diamond-related materials may be of interest as ultrafast field emitters due to their unique band structures.

The successful demonstration of the excellent field emission of diamond and other related materials has led to the study of various wide-bandgap semiconductors,<sup>[87]</sup> including ZnO,<sup>[88]</sup>  $WO_3$ ,<sup>[89]</sup> AlN,<sup>[90]</sup> SiC,<sup>[91]</sup> GaN,<sup>[92]</sup> BN,<sup>[93]</sup> and  $SnO_2$ .<sup>[94]</sup> When nanostructured, these materials offer varied and unique emission properties. Among them, ZnO has been perhaps the most extensively studied, probably due to its ease of synthesis into tipped nanostructures at relatively low temperatures via hydrothermal processing, although vapor phase deposition methods



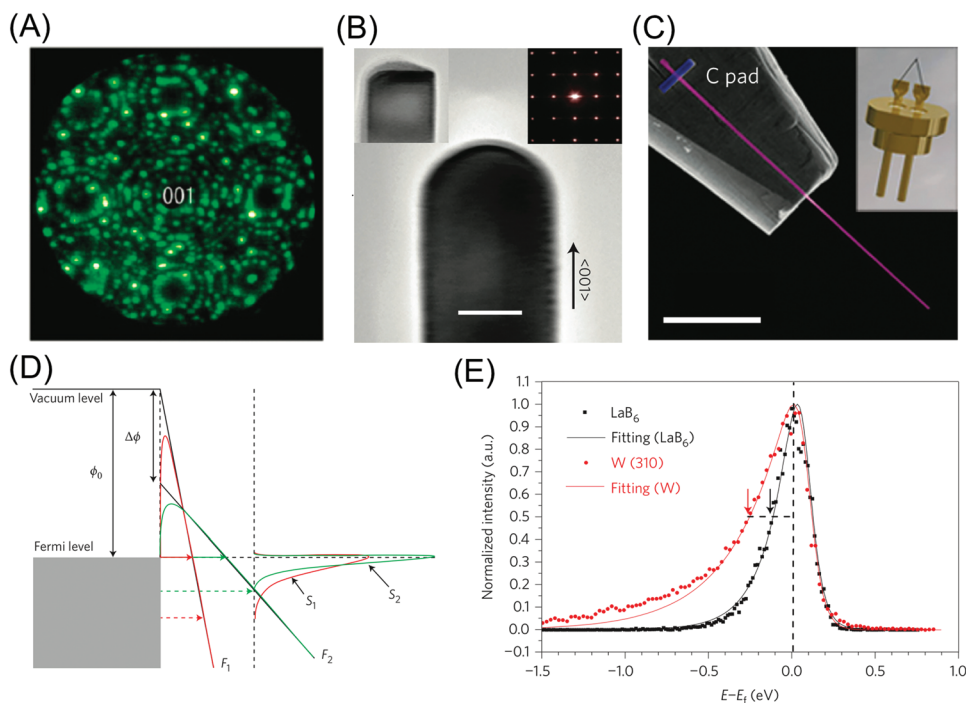


**Figure 6.** LaB<sub>6</sub> nanowire field emitter. A) Field ion microscopy image of a  $\langle 001 \rangle$ -oriented LaB<sub>6</sub> nanowire tip. The pattern shows fourfold symmetry, which agrees with the  $\langle 001 \rangle$  projection stereograph of the LaB<sub>6</sub> crystal. Reproduced with permission.<sup>[101]</sup> Copyright 2010, the American Chemical Society. B) Scanning electron microscopy (SEM) image showing the finished LaB<sub>6</sub> nanowire emitter and the complete emitter assembly used for field-emission SEM. C) Hemispherical nanowire tip produced by field evaporation. Scale bar: 30 nm. Left inset: assembled tip. Right inset: the electron diffraction pattern of the tip after field evaporation, showing that perfect crystallinity is maintained. D) Energy band showing the origin of the low work function of a LaB<sub>6</sub> nanowire and its influence on emission current density and beam monochromaticity. E) Electron energy distribution from a LaB<sub>6</sub> nanowire and a W(310) tip emitting at current densities of  $1.8 \times 10^{10}$  and  $3.6 \times 10^9 \text{ A m}^{-2}$ , respectively. (B–E) Reproduced with permission.<sup>[102]</sup> Copyright 2015, Nature Publishing Group.

have also been widely adopted. Since 2002, the various sharp morphologies that can be produced by ZnO have been widely studied, ranging from tetrapods to nanowires.<sup>[95]</sup>

#### 4.2. Low-Work-Function Materials

Perhaps the most successful low-work-function material to date is lanthanum hexaboride (LaB<sub>6</sub>), which is widely used in both conventional electron microscopy and ultrafast electron microscopy, although other established materials include RuO<sub>2</sub><sup>[96]</sup> and Cs.<sup>[97]</sup> Research on the use of LaB<sub>6</sub> as a field-emitter material has been ongoing since the 1960s.<sup>[98]</sup> As a cold field emitter, LaB<sub>6</sub> nanowires offer a high emission current density, mainly due to their low dimensionality and low work function ( $\approx 2.6 \text{ eV}$ ), as well as their excellent electrical, thermal, and mechanical properties. Compared with a conventional W emitter, a LaB<sub>6</sub> emitter has a lower work function ( $\approx 2.6 \text{ eV}$ ) and higher conductivity. In addition, the hardness of LaB<sub>6</sub> is 5–10 times higher than that of W, possibly improving the damage threshold under a high electric field or an intense laser.<sup>[99]</sup> Field emission from a single LaB<sub>6</sub> nanowire<sup>[100]</sup> shows a very high emission current density of  $5 \times 10^5 \text{ A cm}^{-2}$ . Notably, LaB<sub>6</sub> nanowires with different crystal orientations<sup>[101]</sup> have different field-emission performances. As indicated by the field ion microscopy image in **Figure 6A**, the  $\langle 001 \rangle$ -oriented LaB<sub>6</sub> nanowire emitter shows the highest field-emission crystallographic symmetry—the field-emission sites

are symmetrically distributed on the tip apex, which is expected to provide high stability and reliability.<sup>[101]</sup> The  $\langle 012 \rangle$ -oriented LaB<sub>6</sub> nanowire has the lowest work function ( $\approx 2.4 \text{ eV}$ ) and thus possesses high field-emission intensity and low emission energy spread.<sup>[101]</sup> Recently, the performance of the  $\langle 001 \rangle$ -oriented LaB<sub>6</sub> nanowire (**Figure 6B**) employed as a field-emission electron source (**Figure 6C**) in a scanning electron microscope<sup>[102]</sup> was systematically investigated. Because of the low work function, the required electric field was greatly reduced. The low driving field creates a more rapid decay of the tunneling probability with respect to the energy level below the Fermi level and results in a narrower energy distribution with a higher monochromaticity (**Figure 6D**). Thus, compared with that from conventional W tips, the energy spread of the electrons emitted from a LaB<sub>6</sub> nanowire is reduced considerably (**Figure 6E**). All these factors make LaB<sub>6</sub> nanowires promising ultrafast field emitters.

#### 4.3. 2D Materials

In the late 2000s, 2D materials came to the fore in electron emission research. 2D materials are of interest for field-emission applications due to their atomic scale thickness. This property produces an extremely high aspect ratio at their edges and thus a high field-enhancement factor. As the first widely studied 2D material, graphene was the focus of much interest

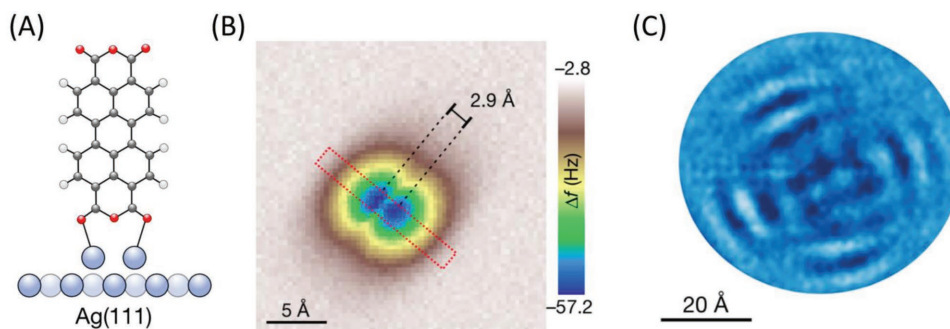


**Figure 7.** Single-molecule field emitter. A) Schematic side view of a standing 3,4,9,10-perylenetetracarboxylic-dianhydride (PTCDA) molecule. B) AFM image of the standing molecule, recorded at  $z = 17.5 \text{ \AA}$ . C) Successive field-emission images (without the background). (A–C) Reproduced with permission.<sup>[12]</sup> Copyright 2018, Springer Nature.

in this context. Graphene is a single layer of carbon atoms arranged in hexagonal lattices and is well known for its breadth of possible applications due to its excellent thermal, mechanical, and electrical properties.<sup>[103]</sup> Similarly, 2D transition-metal dichalcogenides (TMDs), such as  $\text{MoS}_2$ ,<sup>[104]</sup> have also attracted much interest as field emitters. Similar to graphene, 2D TMDs possess atomically sharp edges, enhancing the local electric field and thus facilitating field emission.

However, 2D materials normally lie on a substrate, making it less likely that high field enhancement for field emission can be achieved. One strategy used to overcome this limitation is structuring the graphene edges out of the substrate plane.<sup>[105]</sup> For example, Cheng and co-workers<sup>[106]</sup> used an electrophoretic deposition technique to fabricate homogeneous single-layer graphene films with protruding edges, which showed excellent field-emission properties. A turn-on field (normally defined as the electric field required to produce an emission current density of  $1 \mu\text{A cm}^{-2}$ ) of  $2.3 \text{ V } \mu\text{m}^{-1}$  and a large field-enhancement factor of 3700 were obtained, along with good emission stability and uniformity. Recently, Lyashenko et al.<sup>[22]</sup> presented a study of femtosecond laser-assisted field emission from vertically aligned graphene films, which indicated graphene as a promising ultrafast field emitter. The experimental results can be explained by the two-temperature model considering laser heating of the electrons and energy exchange with the lattice. Li et al.<sup>[107]</sup> reported the field-emission properties of  $\text{MoS}_2$  nanoflowers, exhibiting a turn-on field of  $4.5\text{--}5.5 \text{ V } \mu\text{m}^{-1}$ . Kashid et al.<sup>[108]</sup> investigated the field-emission performance of few-layer  $\text{MoS}_2$ , which showed a turn-on field of  $\approx 3.5 \text{ V } \mu\text{m}^{-1}$ .

Another strategy is the transfer of 2D materials onto sharp nanotips, such as metal nanotips and silicon nanowires, to localize and enhance the electric field.<sup>[109]</sup> Such hybrid structures maintain the field-enhancement factor of the original nanotips due to the atomic thickness of the 2D materials. Recently, Khurshid and co-workers<sup>[13]</sup> used a few-layer graphene-coated Ni wire point cathode to demonstrate the possibility of obtaining stable field emission for electron microscopy and lithography applications under high-vacuum (HV) conditions. The hybrid nanotip has an ultralow work function of  $1.1 \text{ eV}$ ,<sup>[13]</sup> which enables the use of large tips and relatively poor vacuum conditions. This strategy is particularly suitable for point electron source applications, such as electron microscopy.

#### 4.4. Molecular-Scale Emitters

Diamondoids are nanoscale diamond molecules that possess many interesting and unusual optoelectronic properties. They are interesting candidates for field emission because they represent the ultimate limit of the reduction in the grain size of diamond, which has a negative electron affinity.<sup>[110]</sup> More importantly, the conductivity issue of bulk diamond can be avoided by functionalizing metal surfaces with self-assembled monolayers (SAMs) of molecular-scale diamondoids. Researchers have demonstrated that SAMs of diamondoids on metal substrates readily emit electrons with a very narrow kinetic<sup>[111]</sup> energy distribution. This behavior is exactly what is required in electron emission devices such as ultrafast electron microscopes. Recently, Melosh and co-workers<sup>[14]</sup> found that monolayers of diamondoids can effectively confer significantly enhanced field-emission properties to metal surfaces, which was attributed to a reduction in the work function. The four-cage tetramantane–thiol monolayers can reduce the work function of Au to  $1.6\text{--}1.7 \text{ eV}$  due to the formation of excited-state radical cations.<sup>[14]</sup> The authors proposed a new approach for modulating the surface work function, in which nanomaterials that form persistent radical cations are used rather than relying on reactive metals such as Cs or Ru.

As the field of nanomaterials continues to develop, it is becoming increasingly feasible to manufacture single-atom and single-molecule field-emission sources. Most recently, Esat et al.<sup>[12]</sup> reported a new molecular-prylon emitter (Figure 7A,B)—a single molecule (3,4,9,10-perylenetetracarboxylic-dianhydride, PTCDA) standing on a metal surface. The molecule is mounted vertically aligned on a metal tip with sub-nanometer precision and manipulated using scanning tunneling microscopy. The contact between the molecule and metal surface shows high stability,<sup>[112]</sup> which enables the system to function as a coherent single electron field emitter (Figure 7C). The method opens the possibility for the design of functional nanostructures on surfaces.

## 5. Conclusions and Outlook

Ultrafast field emission from nanomaterials is emerging as a very interesting topic in the sense that it extends our

understanding of novel ultrafast electron dynamics beyond the conventional. The general picture of the physics of ultrafast electron emission has already taken shape due to the use of metallic nanotips. However, for emerging materials with distinctive electronic structures and properties, the established framework must be revised and extended. This work is likely to be marked by novel phenomena that can enhance device performance. For instance, along with the high-precision tuning of the electronic structure of CNTs by chirality, chemical doping, and electrical gating, there will be other important adjustable factors for novel OFE electron dynamics that will require careful consideration. Greatly reducing the emitter surface work function is another alternative means of facilitating access to OFE, which has proven of interest to many researchers, particularly regarding work on LaB<sub>6</sub>, diamond, and other wide-bandgap materials. These band structures will of course trigger novel inter- and intraband electron dynamics,<sup>[46,113]</sup> which greatly influence emission performance and as such warrant additional broad study. Furthermore, 2D layered materials have already displayed distinctive nonlinear optics and electronic properties,<sup>[114]</sup> such as spin/valleytronics, and this development is significant for the next generation of spin-polarized ultrafast electron sources. In the pursuit of quiver-quenched OFE, an extremely small emitting tip is preferred because it has an extremely short near-field decay length. To date, single-wall CNTs are one of the few materials suited for such a purpose, given that their emission sites are mainly located at ultrasmall features such as defects. In the same way, single-atom/single-molecule or single-atomic-layer-based emitters also qualify in this regard.

Because of all the advantages of these potential ultrafast field-emission materials, it is possible to generate attosecond precision electron pulses with a high degree of synchronization with the incident optical waveform.<sup>[42]</sup> Not only does this advancement improve time-resolved electron characterization technology to allow attosecond-Angstrom resolution, but it also provides attosecond control and a measurement methodology for electronic systems.<sup>[43]</sup> The future of this relatively new field is likely to be bright indeed, with the next few years revealing not only new theoretical discoveries but also some exciting new technological applications.

## Acknowledgements

S.Z. and K.C. contributed equally to this work. The authors acknowledge funding from the National Key R&D Program of China (Grant No. 2016YFA0202001), and the National Natural Science Foundation of China (Grant Nos. 11427808 and 51602071). Q.D. also benefited from input from many international collaborators, specifically Prof. Kaihui Liu at Peking University, Prof. Zhipei Sun at Aalto University, Prof. Sheng Meng at the Institute of Physics of the Chinese Academy of Sciences, and Prof. Jiayu Dai and Prof. Xiaowei Wang at the National University of Defense Technology.

## Conflict of Interest

The authors declare no conflict of interest.

## Keywords

carbon nanotubes, field emission, graphene, lightwave electronics, optical field emission, ultrafast electron sources

Received: September 9, 2018

Revised: November 29, 2018

Published online:

- [1] N. S. Xu, S. E. Huq, *Mater. Sci. Eng., R* **2005**, *48*, 47.
- [2] a) W. B. Choi, D. S. Chung, J. H. Kang, H. Y. Kim, Y. W. Jin, I. T. Han, Y. H. Lee, J. E. Jung, N. S. Lee, G. S. Park, J. M. Kim, *Appl. Phys. Lett.* **1999**, *75*, 3129; b) Q. H. Wang, A. A. Setlur, J. M. Lauerhaas, J. Y. Dai, E. W. Seelig, R. P. H. Chang, *Appl. Phys. Lett.* **1998**, *72*, 2912.
- [3] a) D. R. Whaley, B. M. Gannon, C. R. Smith, C. M. Armstrong, C. A. Spindt, *IEEE Trans. Plasma Sci.* **2000**, *28*, 727; b) W. I. Milne, K. B. K. Teo, E. Minoux, O. Groening, L. Gangloff, L. Hudanski, J. P. Schnell, D. Dieumegard, F. Peauger, I. Y. Y. Bu, M. S. Bell, P. Legagneux, G. Hasko, G. A. J. Amaratunga, *J. Vac. Sci. Technol., B: Microelectron. Nanometer Struct.–Process., Meas., Phenom.* **2006**, *24*, 345.
- [4] R. Aihara, H. Saito, H. Kohinata, K. Ogura, H. Otsugi, *J. Electron. Microsc.* **1978**, *27*, 353.
- [5] a) G. Cao, Y. Z. Lee, R. Peng, Z. Liu, R. Rajaram, X. Calderon-Colon, L. An, P. Wang, T. Phan, S. Sultana, D. S. Lalush, J. P. Lu, O. Zhou, *Phys. Med. Biol.* **2009**, *54*, 2323; b) Z. J. Liu, G. Yang, Y. Z. Lee, D. Bordelon, J. P. Lu, O. Zhou, *Appl. Phys. Lett.* **2006**, *89*, 103111.
- [6] W. A. Deheer, A. Chatelain, D. Ugarte, *Science* **1995**, *270*, 1179.
- [7] A. G. Rinzler, J. H. Hafner, P. Nikolaev, L. Lou, S. G. Kim, D. Tomanek, P. Nordlander, D. T. Colbert, R. E. Smalley, *Science* **1995**, *269*, 1550.
- [8] T. Y. Zhai, L. Li, Y. Ma, M. Y. Liao, X. Wang, X. S. Fang, J. N. Yao, Y. Bando, D. Golberg, *Chem. Soc. Rev.* **2011**, *40*, 2986.
- [9] a) H. Niikura, P. B. Corkum, *Adv. At. Mol. Opt. Phys.* **2007**, *54*, 511; b) M. F. Ciappina, J. A. Perez-Hernandez, A. S. Landsman, W. A. Okell, S. Zherebtsov, B. Foerg, J. Schoetz, L. Seiffert, T. Fennel, T. Shaaran, T. Zimmermann, A. Chacon, R. Guichard, A. Zair, J. W. G. Tisch, J. P. Marangos, T. Witting, A. Braun, S. A. Maier, L. Roso, M. Kruger, P. Hommelhoff, M. F. Kling, F. Krausz, M. Lewenstein, *Rep. Prog. Phys.* **2017**, *80*, 054401.
- [10] a) B. Barwick, H. S. Park, O. H. Kwon, J. S. Baskin, A. H. Zewail, *Science* **2008**, *322*, 1227; b) A. Feist, K. E. Echterkamp, J. Schauss, S. V. Yalunin, S. Schaefer, C. Ropers, *Nature* **2015**, *521*, 200; c) A. Ryabov, P. Baum, *Science* **2016**, *353*, 374.
- [11] a) A. Feist, N. Bach, N. R. da Silva, T. Danz, M. Moller, K. E. Priebe, T. Domrose, J. G. Gatzmann, S. Rost, J. Schauss, S. Strauch, R. Bormann, M. Sivilis, S. Schafer, C. Ropers, *Ultramicroscopy* **2017**, *176*, 63; b) D. Ehberger, J. Hammer, M. Eisele, M. Kruger, J. Noe, A. Hoge, P. Hommelhoff, *Phys. Rev. Lett.* **2015**, *114*, 227601.
- [12] T. Esat, N. Friedrich, F. S. Tautz, R. Temirov, *Nature* **2018**, *558*, 573.
- [13] X. Y. Shao, A. Srinivasan, W. K. Ang, A. Khurshed, *Nat. Commun.* **2018**, *9*, 8.
- [14] K. T. Narasimha, C. H. Ge, J. D. Fabbri, W. Clay, B. A. Tkachenko, A. A. Fokin, P. R. Schreiner, J. E. Dahl, R. M. K. Carlson, Z. X. Shen, N. A. Melosh, *Nat. Nanotechnol.* **2016**, *11*, 267.
- [15] L. Iemmo, A. Di Bartolomeo, F. Giubileo, G. Luongo, M. Passacantando, G. Niu, F. Hatami, O. Skibitzki, T. Schroeder, *Nanotechnology* **2017**, *28*, 495705.
- [16] M. Krueger, M. Schenk, P. Hommelhoff, *Nature* **2011**, *475*, 78.
- [17] G. Herink, D. R. Solli, M. Gulde, C. Ropers, *Nature* **2012**, *483*, 190.
- [18] E. Goulielmakis, V. S. Yakovlev, A. L. Cavalieri, M. Uiberacker, V. Pervak, A. Apolonski, R. Kienberger, U. Kleineberg, F. Krausz, *Science* **2007**, *317*, 769.

- [19] a) R. H. Fowler, L. Nordheim, *Proc. R. Soc. London, Ser. A* **1928**, 119, 173; b) E. L. Murphy, R. H. Good, *Phys. Rev.* **1956**, 102, 1464.
- [20] a) C. Li, Z. Li, C. Chen, B. Bai, Q. Dai, *Appl. Phys. Lett.* **2017**, 110, 093105; b) Z. J. Li, B. Bai, C. Li, Q. Dai, *Carbon* **2016**, 96, 641.
- [21] M. V. Moghaddam, P. Yaghoobi, G. A. Sawatzky, A. Nojeh, *ACS Nano* **2015**, 9, 4064.
- [22] D. A. Lyashenko, Y. P. Svirko, M. I. Petrov, A. N. Obraztsov, *J. Eur. Opt. Soc.* **2017**, 13, 4.
- [23] D. Ehberger, J. Hammer, M. Eisele, M. Krueger, J. Noe, A. Hoegeler, P. Hommelhoff, *Phys. Rev. Lett.* **2015**, 114, 227601.
- [24] P. Hommelhoff, C. Kealhofer, M. A. Kasevich, *Phys. Rev. Lett.* **2006**, 97, 247402.
- [25] B. Barwick, C. Corder, J. Strohaber, N. Chandler-Smith, C. Uiterwaal, H. Batelaan, *New J. Phys.* **2007**, 9, 142.
- [26] L. Seiffert, T. Paschen, P. Hommelhoff, T. Fennel, *J. Phys. B: At., Mol. Opt. Phys.* **2018**, 51, 134001.
- [27] a) P. Hommelhoff, Y. Sortais, A. Aghajani-Talesh, M. A. Kasevich, *Phys. Rev. Lett.* **2006**, 96, 077401; b) H. Yanagisawa, C. Hafner, P. Dona, M. Klockner, D. Leuenberger, T. Greber, M. Hengsberger, J. Osterwalder, *Phys. Rev. Lett.* **2009**, 103, 257603.
- [28] L. V. Keldysh, *Sov. Phys. - JETP* **1965**, 20, 1307.
- [29] F. V. Bunkin, M. V. Fedorov, *Sov. Phys. - JETP* **1965**, 21, 896.
- [30] P. Musumeci, L. Cultrera, M. Ferrario, D. Filippetto, G. Gatti, M. S. Gutierrez, J. T. Moody, N. Moore, J. B. Rosenzweig, C. M. Soby, G. Travish, C. Vicario, *Phys. Rev. Lett.* **2010**, 104, 084801.
- [31] M. S. Xue, W. F. Wang, J. F. Ou, F. J. Wang, W. Li, *Appl. Phys. Lett.* **2013**, 102, 243110.
- [32] E. Betzig, J. K. Trautman, *Science* **1992**, 257, 189.
- [33] P. F. Liao, A. Wokaun, *J. Chem. Phys.* **1982**, 76, 751.
- [34] C. Li, X. Zhou, F. Zhai, Z. J. Li, F. R. Yao, R. X. Qiao, K. Chen, M. T. Cole, D. P. Yu, Z. P. Sun, K. H. Liu, Q. Dai, *Adv. Mater.* **2017**, 29, 6.
- [35] R. Bormann, M. Gulde, A. Weismann, S. V. Yalunin, C. Ropers, *Phys. Rev. Lett.* **2010**, 105, 147601.
- [36] P. Dombi, A. Hoerl, P. Racz, I. Marton, A. Truegler, J. R. Krenn, U. Hohenester, *Nano Lett.* **2013**, 13, 674.
- [37] H. Yanagisawa, M. Hengsberger, D. Leuenberger, M. Klockner, C. Hafner, T. Greber, J. Osterwalder, *Phys. Rev. Lett.* **2011**, 107, 087601.
- [38] G. G. Paulus, F. Lindner, H. Walther, A. Baltuska, E. Goulielmakis, M. Lezius, F. Krausz, *Phys. Rev. Lett.* **2003**, 91, 253004.
- [39] T. Wittmann, B. Horvath, W. Helml, M. G. Schatzel, X. Gu, A. L. Cavalieri, G. G. Paulus, R. Kienberger, *Nat. Phys.* **2009**, 5, 357.
- [40] a) G. G. Paulus, F. Grasbon, H. Walther, P. Villoresi, M. Nisoli, S. Stagira, E. Priori, S. De Silvestri, *Nature* **2001**, 414, 182; b) T. Wittmann, B. Horvath, W. Helml, M. G. Schatzel, X. Gu, A. L. Cavalieri, G. G. Paulus, R. Kienberger, *Nat. Phys.* **2009**, 5, 357.
- [41] a) F. Lindner, M. G. Schatzel, H. Walther, A. Baltuska, E. Goulielmakis, F. Krausz, D. B. Milosevic, D. Bauer, W. Becker, G. G. Paulus, *Phys. Rev. Lett.* **2005**, 95, 040401; b) R. Gopal, K. Simeonidis, R. Moshhammer, T. Ergler, M. Duerr, M. Kurka, K. U. Kuehnel, S. Tschuch, C. D. Schroeter, D. Bauer, J. Ullrich, A. Rudenko, O. Herrwerth, T. Uphues, M. Schultze, E. Goulielmakis, M. Uiberacker, M. Lezius, M. F. Kling, *Phys. Rev. Lett.* **2009**, 103, 053001.
- [42] A. Baltuska, T. Udem, M. Uiberacker, M. Hentschel, E. Goulielmakis, C. Gohle, R. Holzwarth, V. S. Yakovlev, A. Scrinzi, T. W. Hansch, F. Krausz, *Nature* **2003**, 421, 611.
- [43] P. B. Corkum, F. Krausz, *Nat. Phys.* **2007**, 3, 381.
- [44] M. T. Hassan, J. S. Baskin, B. Liao, A. H. Zewail, *Nat. Photonics* **2017**, 11, 425.
- [45] a) C. Karnetzky, P. Zimmermann, C. Trummer, C. D. Sierra, M. Worle, R. Kienberger, A. Holleitner, *Nat. Commun.* **2018**, 9, 2471; b) T. Rybka, M. Ludwig, M. F. Schmalz, V. Knittel, D. Bida, A. Leitenstorfer, *Nat. Photonics* **2016**, 10, 667.
- [46] T. Higuchi, C. Heide, K. Ullmann, H. B. Weber, P. Hommelhoff, *Nature* **2017**, 550, 224.
- [47] a) J. D. Cox, A. Marini, F. J. G. de Abajo, *Nat. Commun.* **2017**, 8, 14380; b) S. Han, H. Kim, Y. W. Kim, Y. J. Kim, S. Kim, I. Y. Park, S. W. Kim, *Nat. Commun.* **2016**, 7, 13105.
- [48] a) F. Krausz, M. I. Stockman, *Nat. Photonics* **2014**, 8, 205; b) P. Salieres, *Nat. Photonics* **2017**, 11, 333.
- [49] B. Ahn, J. Schötz, M. Kang, W. A. Okell, S. Mitra, B. Förg, S. Zherebtsov, F. Süßmann, C. Burger, M. Kübel, C. Liu, A. Wirth, E. Di Fabrizio, H. Yanagisawa, D. Kim, B. Kim, M. F. Kling, *APL Photonics* **2017**, 2, 036104.
- [50] F. Schertz, M. Schmelzeisen, M. Kreiter, H.-J. Elmers, G. Schoenhense, *Phys. Rev. Lett.* **2012**, 108, 237602.
- [51] F. Kusa, K. E. Echternkamp, G. Herink, C. Ropers, S. Ashihara, *AIP Adv.* **2015**, 5, 077138.
- [52] M. Lehr, B. Foerster, M. Schmitt, K. Kruger, C. Sonnichsen, G. Schonhense, H.-J. Elmers, *Nano Lett.* **2017**, 17, 6606.
- [53] W. P. Putnam, R. G. Hobbs, P. D. Keathley, K. K. Berggren, F. X. Kaertner, *Nat. Phys.* **2017**, 13, 335.
- [54] S. Thomas, G. Wachter, C. Lemell, J. Burgdoerfer, P. Hommelhoff, *New J. Phys.* **2015**, 17, 063010.
- [55] M. Krueger, S. Thomas, M. Foerster, P. Hommelhoff, *J. Phys. B: At., Mol. Opt. Phys.* **2014**, 47, 124022.
- [56] M. E. Swanwick, P. D. Keathley, A. Fallahi, P. R. Krogen, G. Laurent, J. Moses, F. X. Kaertner, L. F. Velasquez-Garcia, *Nano Lett.* **2014**, 14, 5035.
- [57] M. R. Bionta, S. J. Weber, I. Blum, J. Mauchain, B. Chatel, B. Chalopin, *New J. Phys.* **2016**, 18, 103010.
- [58] S. Zherebtsov, T. Fennel, J. Plenge, E. Antonsson, I. Znakovskaya, A. Wirth, O. Herrwerth, F. Suessmann, C. Peltz, I. Ahmad, S. A. Trushin, V. Pervak, S. Karsch, M. J. J. Vrakking, B. Langer, C. Graf, M. I. Stockman, F. Krausz, E. Ruehl, M. F. Kling, *Nat. Phys.* **2011**, 7, 656.
- [59] L. Seiffert, P. Henning, P. Rupp, S. Zherebtsov, P. Hommelhoff, M. F. Kling, T. Fennel, *J. Mod. Opt.* **2017**, 64, 1096.
- [60] Q. Sun, K. Ueno, H. Yu, A. Kubo, Y. Matsuo, H. Misawa, *Light: Sci. Appl.* **2013**, 2, e118.
- [61] M. Siviş, N. Pazos-Perez, R. Yu, R. Alvarez-Puebla, F. J. García de Abajo, C. Ropers, *Commun. Phys.* **2018**, 1, 13.
- [62] a) R. G. Hobbs, W. P. Putnam, A. Fallahi, Y. Yang, F. X. Kaertner, K. K. Berggren, *Nano Lett.* **2017**, 17, 6069; b) P. Racz, Z. Papa, I. Marton, J. Budai, P. Wrobel, T. Stefaniuk, C. Priet, J. R. Krenn, P. Dombi, *Nano Lett.* **2017**, 17, 1181.
- [63] M. E. Swanwick, P. D. Keathley, A. Fallahi, P. R. Krogen, G. Laurent, J. Moses, F. X. Kaertner, L. F. Velasquez-Garcia, *Nano Lett.* **2014**, 14, 5035.
- [64] R. G. Hobbs, Y. Yang, A. Fallahi, P. D. Keathley, E. De Leo, F. X. Kaertner, W. S. Graves, K. K. Berggren, *ACS Nano* **2014**, 8, 11474.
- [65] M. Schenk, M. Krueger, P. Hommelhoff, *Phys. Rev. Lett.* **2010**, 105, 257601.
- [66] M. Kruger, M. Schenk, M. Forster, P. Hommelhoff, *J. Phys. B: At., Mol. Opt. Phys.* **2012**, 45, 074006.
- [67] R. G. Hobbs, Y. Yang, P. D. Keathley, M. E. Swanwick, L. F. Velasquez-Garcia, F. X. Kaertner, W. S. Graves, K. K. Berggren, *Nanotechnology* **2014**, 25, 465304.
- [68] C. Li, X. Zhou, F. Zhai, Z. Li, F. Yao, R. Qiao, K. Chen, D. Yu, Z. Sun, K. Liu, Q. Dai, *Appl. Phys. Lett.* **2017**, 111, 133101.
- [69] P. B. Corkum, *Phys. Rev. Lett.* **1993**, 71, 1994.
- [70] K. E. Echternkamp, G. Herink, S. V. Yalunin, K. Rademann, S. Schafer, C. Ropers, *Appl. Phys. B* **2016**, 122, 10.
- [71] H. Yanagisawa, S. Schnepp, C. Hafner, M. Hengsberger, D. E. Kim, M. F. Kling, A. Landsman, L. Gallmann, J. Osterwalder, *Sci. Rep.* **2016**, 6, 35877.



- [72] a) C. Lemell, X. M. Tong, F. Krausz, J. Burgdorfer, *Phys. Rev. Lett.* **2003**, *90*, 076403; b) M. I. Stockman, P. Hewageegana, *Appl. Phys.* **2007**, *89*, 247.
- [73] a) A. Apolonski, P. Dombi, G. G. Paulus, M. Kakehata, R. Holzwarth, T. Udem, C. Lemell, K. Torizuka, J. Burgdorfer, T. W. Hansch, F. Krausz, *Phys. Rev. Lett.* **2004**, *92*, 073902; b) P. Racz, S. E. Irvine, M. Lenner, A. Mitrofanov, A. Baltuska, A. Y. Elezzabi, P. Dombi, *Appl. Phys. Lett.* **2011**, *98*, 111116.
- [74] B. Piglosiewicz, *Nat. Photonics* **2014**, *8*, 79.
- [75] E. Quinonez, J. Handali, B. Barwick, *Rev. Sci. Instrum.* **2013**, *84*, 103710.
- [76] A. R. Bainbridge, C. W. B. Myers, W. A. Bryan, *Struct. Dyn.* **2016**, *3*, 16.
- [77] M. Gulde, S. Schweda, G. Storeck, M. Maiti, H. K. Yu, A. M. Wodtke, S. Schafer, C. Ropers, *Science* **2014**, *345*, 200.
- [78] M. Muller, A. Paarmann, R. Ernstorfer, *Nat. Commun.* **2014**, *5*, 8.
- [79] F. Suessmann, L. Seiffert, S. Zharebtsov, V. Mondes, J. Stierle, M. Arbeiter, J. Plenge, P. Rupp, C. Peltz, A. Kessel, S. A. Trushin, B. Ahn, D. Kim, C. Graf, E. Ruehl, M. F. Kling, T. Fennel, *Nat. Commun.* **2015**, *6*, 7944.
- [80] L. Seiffert, Q. Liu, S. Zharebtsov, A. Trabattori, P. Rupp, M. C. Castrovillani, M. Galli, F. Suessmann, K. Wintersperger, J. Stierle, G. Sansone, L. Poletto, F. Frassetto, I. Halfpap, V. Mondes, C. Graf, E. Ruehl, F. Krausz, M. Nisoli, T. Fennel, F. Calegari, M. F. Kling, *Nat. Phys.* **2017**, *13*, 766.
- [81] H. Li, B. Mignolet, G. Wachter, S. Skruszewicz, S. Zharebtsov, F. Suessmann, A. Kessel, S. A. Trushin, N. G. Kling, M. Kuebel, B. Ahn, D. Kim, I. Ben-Itzhak, C. L. Cocke, T. Fennel, J. Tiggesbaumer, K. H. Meiwes-Broer, C. Lemell, J. Burgdorfer, R. D. Levine, F. Remacle, M. F. Kling, *Phys. Rev. Lett.* **2015**, *114*, 123004.
- [82] M. W. Geis, N. N. Efremow, J. D. Woodhouse, M. D. McAleese, M. Marchywka, D. G. Socker, J. F. Hochedez, *IEEE Electron Device Lett.* **1991**, *12*, 456.
- [83] J. Vanderweide, Z. Zhang, P. K. Baumann, M. G. Wensell, J. Bernholz, R. J. Nemanich, *Phys. Rev. B* **1994**, *50*, 5803.
- [84] N. G. Shang, P. Papakonstantinou, P. Wang, A. Zakharov, U. Palnitkar, I. N. Lin, M. Chu, A. Stamboulis, *ACS Nano* **2012**, *6*, 7540.
- [85] T. Tyler, V. V. Zhirnov, A. V. Kvit, D. Kang, J. J. Hren, *Appl. Phys. Lett.* **2003**, *82*, 2904.
- [86] V. Porshyn, V. I. Kleshch, E. A. Obratsova, A. L. Chuvilin, D. Lutzenkirchen-Hecht, A. N. Obratsov, *Appl. Phys. Lett.* **2017**, *110*, 182101.
- [87] W. K. Yi, T. Jeong, S. G. Yu, J. Heo, C. Lee, J. Lee, W. Kim, J. B. Yoo, J. Kim, *Adv. Mater.* **2002**, *14*, 1464.
- [88] F. H. Chu, C. W. Huang, C. L. Hsin, C. W. Wang, S. Y. Yu, P. H. Yeh, W. W. Wu, *Nanoscale* **2012**, *4*, 1471.
- [89] F. Liu, L. Li, F. Y. Mo, J. Chen, S. Z. Deng, N. S. Xu, *Cryst. Growth Des.* **2010**, *10*, 5193.
- [90] J. H. He, R. S. Yang, Y. L. Chueh, L. J. Chou, L. J. Chen, Z. L. Wang, *Adv. Mater.* **2006**, *18*, 650.
- [91] Z. W. Pan, H. L. Lai, F. C. K. Au, X. F. Duan, W. Y. Zhou, W. S. Shi, N. Wang, C. S. Lee, N. B. Wong, S. T. Lee, S. S. Xie, *Adv. Mater.* **2000**, *12*, 1186.
- [92] B. D. Liu, Y. Bando, C. C. Tang, F. F. Xu, J. Q. Hu, D. Golberg, *J. Phys. Chem. B* **2005**, *109*, 17082.
- [93] X. X. Yang, Z. J. Li, F. He, M. J. Liu, B. Bai, W. Liu, X. Qiu, H. Zhou, C. Li, Q. Dai, *Small* **2015**, *11*, 3710.
- [94] H. Chi, H. C. Zhu, H. J. Xu, X. D. Shan, Z. M. Liao, D. P. Yu, *J. Phys. Chem. C* **2009**, *113*, 6450.
- [95] a) Y. F. Li, Z. P. Zhang, G. F. Zhang, L. Zhao, S. Z. Deng, N. S. Xu, J. Chen, *ACS Appl. Mater. Interfaces* **2017**, *9*, 3911; b) Z. P. Zhang, X. M. Song, Y. C. Chen, J. C. She, S. Z. Deng, N. S. Xu, J. Chen, *J. Alloys Compd.* **2017**, *690*, 304.
- [96] C. L. Cheng, Y. F. Chen, R. S. Chen, Y. S. Huang, *Appl. Phys. Lett.* **2005**, *86*, 103104.
- [97] D. H. Kim, H. R. Lee, M. W. Lee, J. H. Lee, Y. H. Song, J. G. Jee, S. Y. Lee, *Chem. Phys. Lett.* **2002**, *355*, 53.
- [98] a) E. E. Windsor, *Proc. Inst. Electr. Eng.* **1969**, *116*, 348; b) M. Futamoto, S. Hosoki, H. Okano, U. Kawabe, *J. Appl. Phys.* **1977**, *48*, 3541; c) H. Nagata, K. Harada, R. Shimizu, *J. Appl. Phys.* **1990**, *68*, 3614; d) K. C. Qi, Z. L. Lin, W. B. Chen, G. C. Cao, J. B. Cheng, X. W. Sun, *Appl. Phys. Lett.* **2008**, *93*, 093503; e) M. Nakamoto, K. Fukuda, *Appl. Surf. Sci.* **2002**, *202*, 289.
- [99] a) H. Zhang, J. Tang, L. Zhang, B. An, L.-C. Qin, *Appl. Phys. Lett.* **2008**, *92*, 173121; b) M. Futamoto, T. Aita, U. Kawabe, *Mater. Res. Bull.* **1979**, *14*, 1329; c) V. V. Morozov, V. I. Malnev, S. N. Dub, P. I. Loboda, V. S. Kresanov, *Inorg. Mater.* **1984**, *20*, 1225; d) G. Herink, L. Wimmer, C. Ropers, *New J. Phys.* **2014**, *16*, 123005.
- [100] H. Zhang, J. Tang, Q. Zhang, G. P. Zhao, G. Yang, J. Zhang, O. Zhou, L. C. Qin, *Adv. Mater.* **2006**, *18*, 87.
- [101] H. Zhang, J. Tang, J. Yuan, J. Ma, N. Shinya, K. Nakajima, H. Murakami, T. Ohkubo, L. C. Qin, *Nano Lett.* **2010**, *10*, 3539.
- [102] H. Zhang, J. Tang, J. S. Yuan, Y. Yamauchi, T. T. Suzuki, N. Shinya, K. Nakajima, L. C. Qin, *Nat. Nanotechnol.* **2016**, *11*, 273.
- [103] a) A. A. Balandin, S. Ghosh, W. Bao, I. Calizo, D. Teweldebrhan, F. Miao, C. N. Lau, *Nano Lett.* **2008**, *8*, 902; b) A. K. Geim, K. S. Novoselov, *Nat. Mater.* **2007**, *6*, 183; c) K. S. Novoselov, A. K. Geim, S. V. Morozov, D. Jiang, M. I. Katsnelson, I. V. Grigorieva, S. V. Dubonos, A. A. Firsov, *Nature* **2005**, *438*, 197.
- [104] a) B. Radisavljevic, A. Radenovic, J. Brivio, V. Giacometti, A. Kis, *Nat. Nanotechnol.* **2011**, *6*, 147; b) Z. Yin, H. Li, H. Li, L. Jiang, Y. Shi, Y. Sun, G. Lu, Q. Zhang, X. Chen, H. Zhang, *ACS Nano* **2012**, *6*, 74; c) A. Castellanos-Gomez, M. Poot, G. A. Steele, H. S. J. van der Zant, N. Agrait, G. Rubio-Bollinger, *Nanoscale Res. Lett.* **2012**, *7*, 233; d) K. F. Mak, C. Lee, J. Hone, J. Shan, T. F. Heinz, *Phys. Rev. Lett.* **2010**, *105*, 136805.
- [105] a) N. G. Shang, C. P. Li, W. K. Wong, C. S. Lee, I. Bello, S. T. Lee, *Appl. Phys. Lett.* **2002**, *81*, 5024; b) A. N. Obratsov, A. P. Volkov, A. A. Zakhidov, D. A. Lyashenko, Y. V. Petrushenko, O. P. Satanovskaya, *Appl. Surf. Sci.* **2003**, *215*, 214; c) J. J. Wang, M. Y. Zhu, R. A. Outlaw, X. Zhao, D. M. Manos, B. C. Holloway, V. P. Mamma, *Appl. Phys. Lett.* **2004**, *85*, 1265; d) J. J. Wang, M. Y. Zhu, X. Zhao, R. A. Outlaw, D. M. Manos, B. C. Holloway, C. Park, T. Anderson, V. P. Mamma, *J. Vac. Sci. Technol., B: Microelectron. Nanometer Struct. – Process., Meas., Phenom.* **2004**, *22*, 1269; e) S. K. Srivastava, A. K. Shukla, V. Vankar, V. Kumar, *Thin Solid Films* **2005**, *492*, 124; f) M. Y. Chen, C. M. Yeh, J. S. Syu, J. Hwang, C. S. Kou, *Nanotechnology* **2007**, *18*, 185706; g) G. Eda, H. E. Unalan, N. Rupasinghe, G. A. J. Amaratunga, M. Chhowalla, *Appl. Phys. Lett.* **2008**, *93*, 233502; h) A. Malesevic, R. Kemps, A. Vanhulsel, M. P. Chowdhury, A. Volodin, C. Van Haesendonck, *J. Appl. Phys.* **2008**, *104*, 084301; i) U. A. Palnitkar, R. V. Kashid, M. A. More, D. S. Joag, L. S. Panchakarla, C. N. R. Rao, *Appl. Phys. Lett.* **2010**, *97*, 063102.
- [106] Z. S. Wu, S. F. Pei, W. C. Ren, D. M. Tang, L. B. Gao, B. L. Liu, F. Li, C. Liu, H. M. Cheng, *Adv. Mater.* **2009**, *21*, 1756.
- [107] Y. B. Li, Y. Bando, D. Golberg, *Appl. Phys. Lett.* **2003**, *82*, 1962.
- [108] R. V. Kashid, D. J. Late, S. S. Chou, Y. K. Huang, M. De, D. S. Joag, M. A. More, V. P. Dravid, *Small* **2013**, *9*, 2730.
- [109] a) D. Ye, S. Moussa, J. D. Ferguson, A. A. Baski, M. S. El-Shall, *Nano Lett.* **2012**, *12*, 1265; b) S. Lv, Z. Li, J. Liao, G. Wang, M. Li, W. Miao, *Sci. Rep.* **2015**, *5*, 15035; c) Z. Yang, Q. Zhao, Y. Ou, W. Wang, H. Li, D. Yu, *Appl. Phys. Lett.* **2012**, *101*, 173107; d) A. T. T. Koh, Y. M. Foong, Z. Yusop, M. Tanemura, D. H. C. Chua, *Adv. Mater. Interfaces* **2014**, *1*, 1300147.
- [110] W. Zhu, G. P. Kochanski, S. Jin, *Science* **1998**, *282*, 1471.
- [111] W. L. Yang, J. D. Fabbri, T. M. Willey, J. R. I. Lee, J. E. Dahl, R. M. K. Carlson, P. R. Schreiner, A. A. Fokin, B. A. Tkachenko, N. A. Fokina, W. Meevasana, N. Mannella, K. Tanaka, X. J. Zhou,

- T. van Buuren, M. A. Kelly, Z. Hussain, N. A. Melosh, Z. X. Shen, *Science* **2007**, 316, 1460.
- [112] a) G. Witte, C. Woll, *J. Mater. Res.* **2004**, 19, 1889; b) R. J. Maurer, V. G. Ruiz, J. Camarillo-Cisneros, W. Liu, N. Ferri, K. Reuter, A. Tkatchenko, *Prog. Surf. Sci.* **2016**, 91, 72.
- [113] a) M. Schultze, K. Ramasesha, C. D. Pemmaraju, S. A. Sato, D. Whitmore, A. Gandman, J. S. Prell, L. J. Borja, D. Prendergast, K. Yabana, D. M. Neumark, S. R. Leone, *Science* **2014**, 346, 1348; b) A. Schiffrin, T. Paasch-Colberg, N. Karpowicz, V. Apalkov, D. Gerster, S. Muhlbrandt, M. Korbman, J. Reichert, M. Schultze, S. Holzner, J. V. Barth, R. Kienberger, R. Ernstorfer, V. S. Yakovlev, M. I. Stockman, F. Krausz, *Nature* **2013**, 493, 70.
- [114] A. Autere, H. Jussila, Y. Y. Dai, Y. D. Wang, H. Lipsanen, Z. P. Sun, *Adv. Mater.* **2018**, 30, 1705963.